(Preprint) AAS 17-273

ATMOSPHERIC MODELING USING ACCELEROMETER DATA DURING MARS ATMOSPHERE AND VOLATILE EVOLUTION (MAVEN) FLIGHT OPERATIONS

Robert H. Tolson,[*] Rafael A. Lugo,[†] Darren T. Baird,[‡] Alicia D. Cianciolo,[§] Stephen W. Bougher,[**] and Richard M. Zurek[††]

The Mars Atmosphere and Volatile EvolutioN (MAVEN) spacecraft is a NASA orbiter designed to explore the Mars upper atmosphere, typically from 140 to 160 km altitude. In addition to the nominal science mission, MAVEN has performed several Deep Dip campaigns in which the orbit's closest point of approach, also called periapsis, was lowered to an altitude range of 115 to 135 km. MAVEN accelerometer data were used during mission operations to estimate atmospheric parameters such as density, scale height, along-track gradients, and wave structures. Density and scale height estimates were compared against those obtained from the Mars Global Reference Atmospheric Model and used to aid the MAVEN navigation team in planning maneuvers to raise and lower periapsis during Deep Dip operations. This paper describes the processes used to reconstruct atmosphere parameters from accelerometers data and presents the results of their comparison to model and navigation-derived values.

INTRODUCTION

An atmospheric parameter recovery method has previously been presented and applied to data recorded during the aerobraking phases of the Mars Global Surveyor (MGS), Mars Odyssey (ODY), and Mars Reconnaissance Orbiter (MRO) missions.[1,2,3,4] This method uses spacecraft accelerometer data to estimate atmospheric density along the spacecraft trajectory. The same method was proposed for the Mars Atmosphere and Volatile EvolutioN (MAVEN) mission.[5] Aerobraking missions are typically controlled to keep periapsis within atmospheric density corridors that range from 20-40 kg/km^3. However, the MAVEN nominal science orbits have a density corridor of 0.05-0.15 kg/km^3 and the Deep Dip corridor is 2.5-4.0 kg/km^3. In past missions, the spacecraft attitude during aerobraking is essentially the same from one periapsis pass to another, whereas MAVEN utilizes a number of significantly different attitudes relative to the wind. These operational changes required modifications to the prior approach including introducing along-track density and temperature gradients in the atmospheric model, resorting to a non-linear optimization to obtain a least squares fit to the noisy low-density data, and extending the aerodynamic database to a variety of attitudes. This paper presents this method to recover the atmospheric density profile along the MAVEN spacecraft trajectory as it flies through periapsis.

[*] Professor Emeritus, National Institute of Aerospace, 100 Exploration Way, Hampton VA 23666
[†] Aerospace Engineer, Analytical Mechanics Associates, Inc., Hampton, VA 23666
[‡] Aerospace Engineer, NASA Johnson Space Center, Houston, TX, 77058
[§] Aerospace Engineer, NASA Langley Research Center, Hampton, VA 23666
[**] Professor, Climate and Space Sciences and Engineering Department, University of Michigan, Ann Arbor, MI 48109
[††] Aerospace Engineer, Jet Propulsion Laboratory, California Institute of Technology, Pasadena, CA 91109

MISSION AND SPACECRAFT SUMMARY

MAVEN is a NASA orbiter designed to study the Mars upper atmosphere, ionosphere, their interactions with solar wind, and how these features and phenomena have evolved over time.[6] MAVEN joins two other NASA Mars orbiters currently in operation, MRO and ODY, as well as Mars Express operated by the European Space Agency, and the Mars Orbiter Mission operated by the Indian Space Research Organization.

Mission Profile

The MAVEN spacecraft was launched from Cape Canaveral aboard an Atlas V 401 on November 18, 2013, and entered Mars orbit on September 22, 2014.[7] Nominal science operations began on November 16, 2014. As of December 31, 2016, the spacecraft had successfully completed 4,383 periapsis passes.

MAVEN orbits are categorized into science orbits and Deep Dip (DD) campaigns. Science orbits describe operations during which the minimum altitude at periapsis ranges from 140-180 km. DD campaigns are one-week periods when the spacecraft periapsis altitude is lowered to between 115-135 km to reach a prescribed peak density corridor.[8] At the time of this writing, MAVEN has conducted six DD campaigns. A comparison of the relevant orbit parameters between science and DD orbits is listed in Table 1. Both types of orbits have a 4.5 hour period, a 75° inclination, and an eccentricity of 0.47.[7,8] Note that the observed periapsis densities are outside the targeted corridor bounds. While the navigation team attempted to maintain the vehicle in the targeted corridor based on atmospheric predictions, a combination of atmospheric variability and modeling limitations led to orbits that occasionally exceeded the corridor bounds.

Table 1. Comparison of science and Deep Dip orbit parameters.[7,8]

Orbit Parameter	Nominal Science Orbits	Deep Dip Orbits
Periapsis Altitude	140-180 km	115-135 km
Targeted Periapsis Density	0.05-0.15 kg/km^3	2.00-3.50 kg/km^3
Observed Periapsis Density	0.01-1.00 kg/km^3	1.00-11.00 kg/km^3

Spacecraft

The MAVEN orbiter, shown in Figure 1, is equipped with a variety of science and engineering instrumentation, including the Solar Wind Electron Analyzer (SWEA), the Langmuir Probe and Waves antennae (LPW), the Solar Energetic Particles instrument (SEP), the Solar Wind Ion Analyzer (SWIA), and magnetometers (MAG). The Articulated Payload Platform (APP) is mounted at the end of a boom that is extended away from the spacecraft central structure and houses the Neutral Gas and Ion Mass Spectrometer (NGIMS), the Imaging Ultraviolet Spectrograph (IUVS), and the SupraThermal and Thermal Ion Composition instrument (STATIC). A sun sensor is also mounted on the end of each solar array. The high-gain antenna (HGA) is mounted to the central structure and is non-articulated, meaning that to transmit data back to Earth, the entire spacecraft must be rotated to point towards Earth. Guidance, navigation, and control (GN&C) instrumentation includes two star trackers, four reaction wheels, and two miniature inertial measurement units (MIMU) mounted to the MAVEN central structure. These instruments are illustrated in Figure 2. In the figure, the coordinate frame shown is the spacecraft mechanical frame and is oriented the same as the spacecraft aerodynamic frame discussed later in this paper. The present work focuses primarily on results from flight data obtained from accelerometers located in the MIMU.

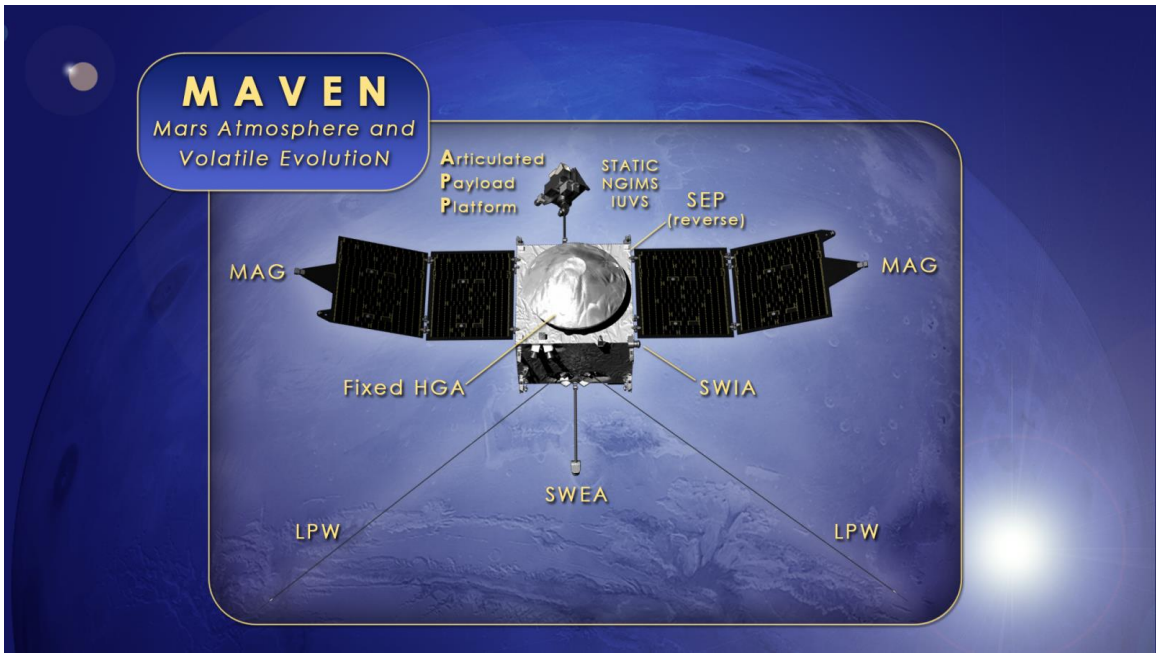

Figure 1. MAVEN spacecraft.[9]

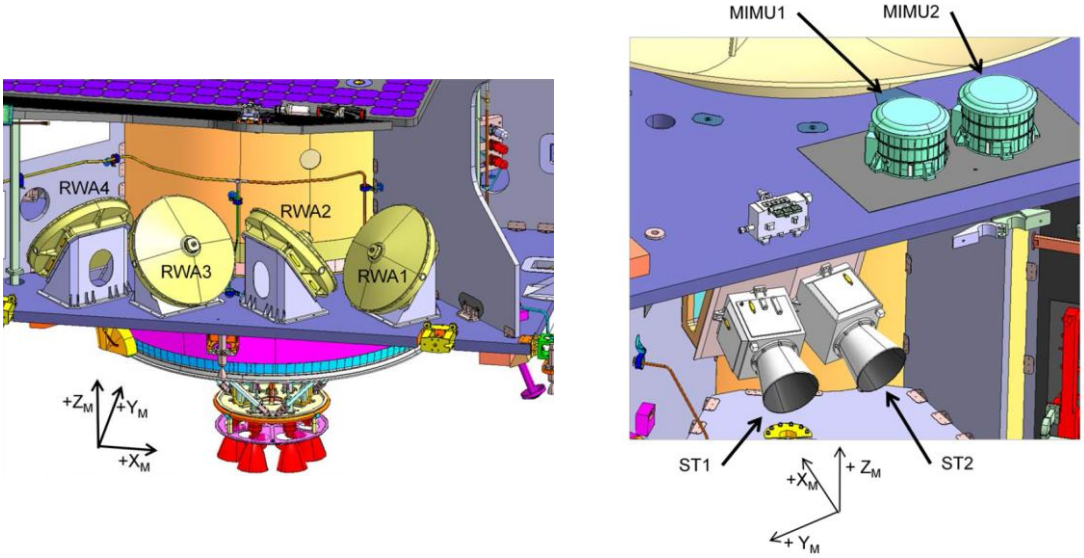

Figure 2. MAVEN reaction wheel assemblies, MIMUs, and star trackers mounted to the MAVEN central structure.[10]

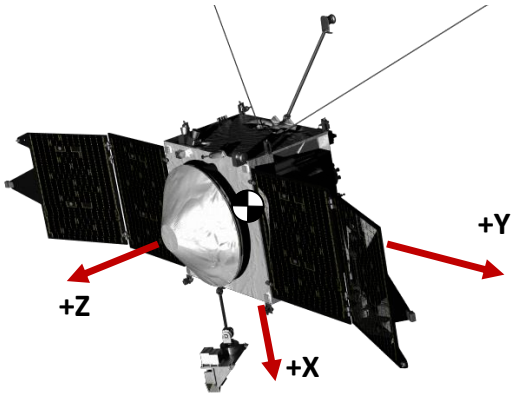

Figure 3. MAVEN body-fixed aerodynamic coordinate frame.

The aerodynamic coordinate frame used in the present analysis is shown in Figure 3. The origin of the frame is fixed to the spacecraft center of mass. The +Z axis is pointed out through the HGA boresight, the +X axis parallel to the APP boom, and the +Y axis is pointed out along the solar array and completes the right-hand orthogonal frame. The APP can be seen towards the bottom of the figure.

Flight Operations

The spacecraft switches between several attitude modes throughout an orbit to provide optimal coverage for different science instruments. During flight operations near periapsis, the vehicle is slewed to a "Fly Z" or "Velocity-Nadir" attitude such that the –Z axis is pointed along the velocity vector and the +X axis is pointed toward nadir (down toward the planet center of mass).[8] This is illustrated in Figure 4, in which the spacecraft is flying left-to-right in a "Fly Z" mode in which the –Z body axis is pointed along the velocity vector. However, some orbits are flown with a "Fly Y" orientation at periapsis. This variation in spacecraft attitude from orbit to orbit is one reason why the previous density recovery method was modified for application to the MAVEN mission.

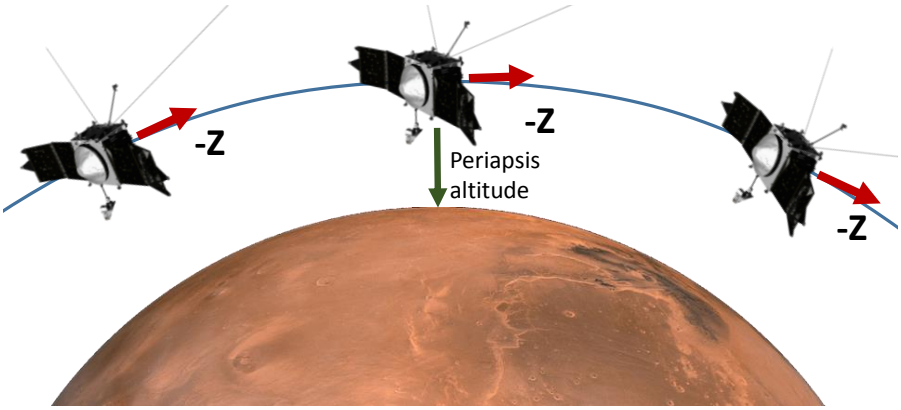

Figure 4. Notional representation of a MAVEN periapsis pass (not to scale).

Data from the spacecraft instruments are telemetered back to Earth and processed by Lockheed Martin Space Systems Company (LMSSC) before being made available to the science teams through the MAVEN Science Data Center (SDC), an online data portal and repository maintained by the Laboratory for Atmospheric and Space Physics at University of Colorado Boulder.[11] Data are posted at regular intervals and downloaded to local drives for further processing and analysis.

The methods presented in this paper were used during DD campaigns to provide daily observations of wave structure phenomena and estimates of peak density and scale height to the MAVEN Atmospheric Advisory Group (AAG). Data were downloaded daily from the SDC and processed. After density profiles and scale heights were estimated, a report was compiled containing plots and tabulated summaries of the results. The report was presented to the AAG and the group formulated a recommendation to the spacecraft navigation (NAV) group regarding the magnitude and direction of upcoming maneuvers based in part on the ACC results.

Aerodynamic Database

To accommodate the various mission phases, the aerodynamic database, used for processing the accelerometer data, was populated with data calculated from two different programs. Direct Simulation Monte Carlo (DSMC) Analysis Code (DAC)[12] was used for DD orbits (free molecular/transitional flow) and FreeMat[13] was used for science orbits (free molecular flow).

During DD campaigns, the aerodynamic flow during a periapsis pass ranges from free molecular to transitional. The database for this phase was generated using DAC. A high-resolution MAVEN spacecraft surface geometry for the DAC simulation was obtained from LMSSC. With one exception, the DAC simulation inputs were the same as those used to develop the project aerodynamic database used by LMSSC and NAV during operations. These similar inputs included a velocity of 4,213 m/s and an atmospheric chemical composition of 95.3% CO_2, 3% N_2, and 1.7% Ar. This composition is reasonable since DD campaigns occur near or slightly above the homopause.

The input exception was the assumed values for the normal and tangential momentum accommodation coefficients. LMSSC assumed that 80% of the gas surface interaction had accommodation coefficients of unity and 20% was a specular reflection. For accelerometer data processing in the present analysis, it was assumed that 100% of the gas surface interaction had complete thermal accommodation, which is consistent with traditional assumptions for previous missions. For a cold flat plate, with normal incidence, this results in the LMSSC database providing a drag coefficient that is approximately 20% larger than the ACC value, thereby resulting in the NAV group obtaining atmospheric density values that were 20% less than ACC (comparisons will be discussed later, see Figure 9). It is expected that future analysis of other available data types, namely mass spectrometer data from NGIMS, will help validate these assumptions. Other data such as reaction wheel data and raw MIMU counts may also provide further insight, but analysis will also depend on thermal accommodation assumptions.

The upper panels of Figure 5 show the drag coefficient for two of the DAC generated data sets selected to bound the nominal DD density corridor. The data in the upper left panel was generated for a freestream density of 4.0 kg/km^3, and the data in the upper right panel was generated for a freestream density of 1.0 kg/km^3. The variables u_x and u_y are the *x* and *y* components of the wind-relative vehicle velocity unit vector in the body aerodynamic frame shown in Figure 3. Thus, the database spans ±11.5° of deviation in the wind-relative velocity vector from the spacecraft Z axis ($\sin^{-1} 0.2 = 11.5°$). Data were generated at five equally-spaced values of u_x and u_y. The maximum C_d is off-center, and is likely due to the APP, SWEA, and LPW structures. MAVEN trims around $u_x = -0.06$ due primarily to the APP and deviates only a small angle from trim during a DD periapsis pass. Two additional data sets include one at a freestream density of 15 kg/km^3 and one generated using the free molecular flow version of DAC, the latter of which is shown in the lower left panel of Figure 5.

The lower right panel of Figure 5 show the drag coefficient at $u_x = u_y = 0$ at several densities for MAVEN (abbreviated here as MVN), MGS, and ODY. Free molecular flow data was unavailable for MGS, so C_d was held constant for extrapolation below 0.1 kg/km^3. In addition to the expected trend of a decrease in drag coefficient as the flow moves towards continuum flow, there is also a noticeable shift in the curves themselves between orbiters. ODY, which had no solar array sweep, exhibits the highest drag coefficients. MGS, which had a 30° sweep of its entire solar array assemblies, exhibits the lowest drag coefficients. MAVEN, which has a 20° sweep of half of its solar arrays, is in between and trends closer to ODY. Such a trend might be expected because in all three cases, the incoming momentum flux is absorbed across the projected area. The emitted flux is normal to the surface area after accommodation, so that the solar array sweep lowers the effect of the emitted flux on the drag coefficient.

The transitional flow effects are also clearly seen in the lower right panel. During atmospheric density recovery, linear interpolation between the four tables is performed using $\log\rho$ as the independent variable. Densities less than 0.001 kg/km^3 use the free molecular value of C_d. Additional data sets were deemed unnecessary as the change in C_d between adjacent sets is approximately 2-3%.

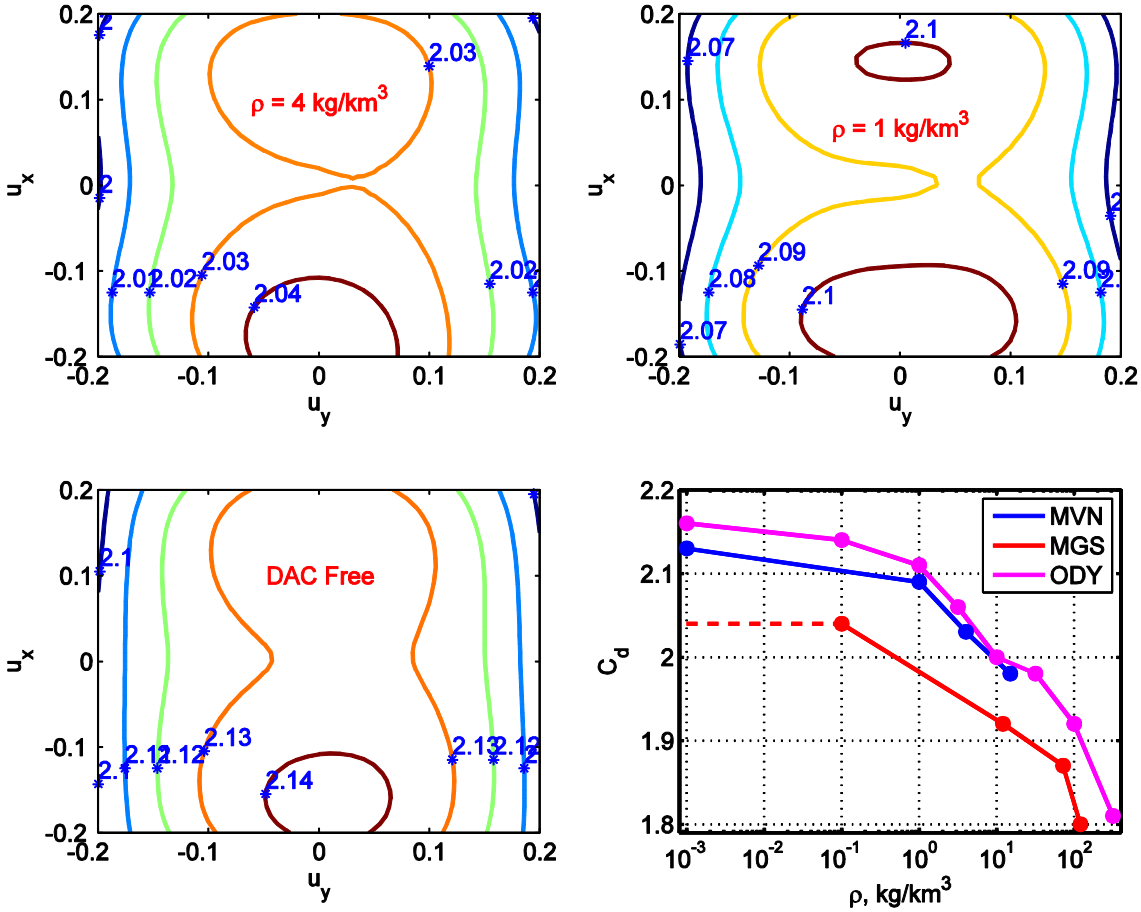

Figure 5. MAVEN drag coefficient derived from DAC simulations used with accelerometer data to recover atmospheric density for DD orbits.

For science orbits, nominal density corridor is from 0.05 to 0.15 kg/km^3. Based on Figure 5, the corridor is sufficiently close to free molecular flow, so that using free molecular flow values will

likely produce less than 2% error. Since numerous attitudes can result during mission operations ("Fly Z" and "Fly Y" flight modes previously mentioned, Earth pointing for communications, and safe mode), a complete 4π steradian data base was generated using 5° grid spacing. The data were generated using FreeMat, in which the surface geometry of the spacecraft is represented by flat rectangular, circular and triangular plates, circular cylinders, frusta of cones, spheres, and spherical caps.

The resulting values of C_d for science orbits generated by FreeMat are shown in Figure 6. Since for each pair (u_x, u_y) there are two solutions for u_z from $u_x^2 + u_y^2 + u_z^2 = 1$, there are two contours. The two contours are very similar because of the near symmetry of MAVEN about the *x*-*z* and the *y*-*z* planes. The smallest C_d is 0.58 and occurs when $u_x = -1$ and $u_y = u_z = 0$, i.e., when the flow is parallel to all solar array surfaces. For flow along the Z axis, $C_d(0.0) = 2.15$, which is within 1% of the value obtained from Free DAC (see Figure 5).

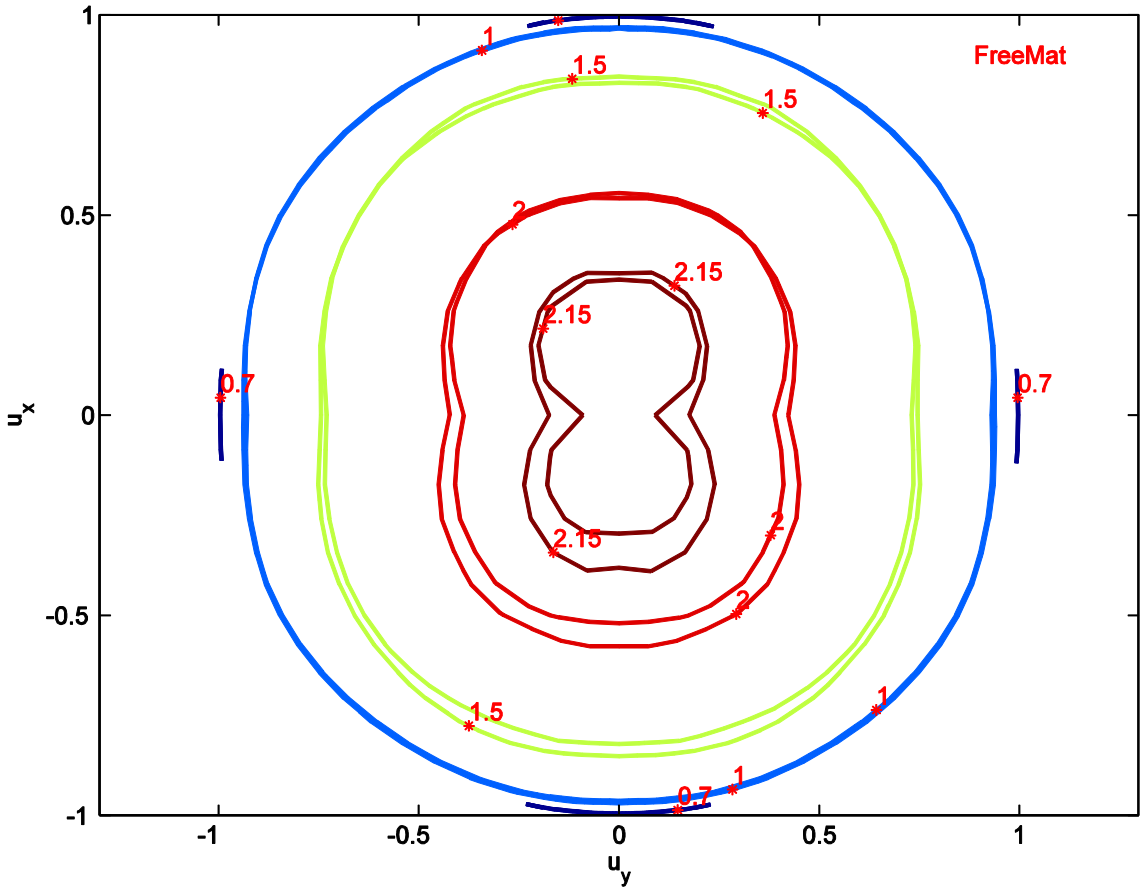

Figure 6. MAVEN drag coefficient derived from free molecular flow simulations used with accelerometer data to recover atmospheric density for nominal science orbits.

Accelerometers and Accelerometer Data

The MAVEN spacecraft carries two Honeywell MIMUs, each containing three orthogonally mounted QA3000 accelerometers and GG1320 ring laser gyroscopes. The measured accelerations $\tilde{\mathbf{a}}$ are described by

$$\tilde{\mathbf{a}} = \mathbf{a}_{\text{bias}} + \mathbf{a}_{\text{aero}} + \mathbf{a}_{\text{grav}} + \mathbf{a}_{\text{ACS}} + \dot{\boldsymbol{\omega}} \times \mathbf{r} + \boldsymbol{\omega} \times (\boldsymbol{\omega} \times \mathbf{r}) \tag{1}$$

where $\mathbf{a}_{bias}$ are the accelerometer biases, $\mathbf{a}_{aero}$ are the accelerations caused by the aerodynamic forces, $\mathbf{a}_{grav}$ are the accelerations caused by gravity gradients, and $\mathbf{a}_{ACS}$ are the accelerations caused by attitude control system thruster firings. The final two terms describe the accelerations caused by the angular motion of the accelerometers about the spacecraft center of mass.

The gravity gradient is negligible, and thrusters are not fired during the ±300 s period centered at periapsis, so the $\mathbf{a}_{grav}$ and $\mathbf{a}_{ACS}$ terms may be ignored. The final two terms in Eq. (1) may be computed and removed using gyroscope data and preflight knowledge of the accelerometer location relative to the spacecraft center of gravity (CG). This transforms the accelerations sensed by the MIMU to those of the spacecraft CG. Although accelerometer biases are computed on-board and removed prior to data delivery, a time-dependent accelerometer bias is computed and removed to account for temperature-induced differences seen in inbound and outbound biases.[5] Thus, Eq. (1) reduces to

$$\mathbf{a}_{CG} = \mathbf{a}_{aero} \tag{2}$$

where $\mathbf{a}_{CG}$ are the accelerations of the spacecraft CG due to aerodynamic forces acting on the spacecraft.

The left panels of Figure 7 show the acceleration data from orbit 1060 used to compute the bias for each axis (note that this data ranges from ±350 s rather than ±300 s; the additional data is to ensure an accurate bias calculation). The right panels show the bias-corrected accelerometer data used to recover density. It can be seen that the accelerometer biases are small, but different, for the inbound and outbound portions of the pass. For this orbit, the *z*-axis shows the largest acceleration magnitude, indicating a "Fly Z" orientation. This correction is applied to each processed periapsis pass.

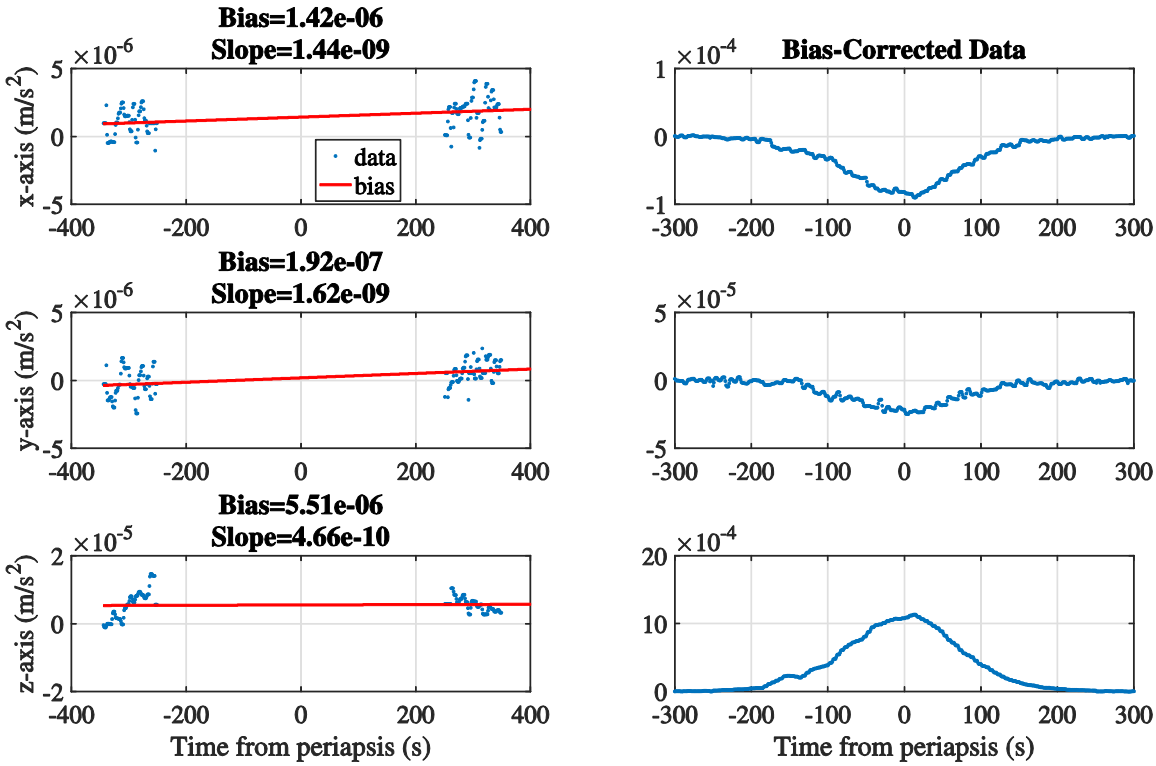

Figure 7. Bias calculation and bias-corrected acceleration data for orbit 1060 (Deep Dip 2).

ATMOSPHERIC DENSITY RECOVERY

Recovery of atmospheric density and related parameters may be broadly described as a two-step process:

1. The freestream atmospheric density profile $\hat{\rho}$ is estimated using accelerometer measurements, the preflight aerodynamic database, and spacecraft state at periapsis. This *estimated density* is used to observe and interpret wave structure and other atmospheric phenomena.
2. The *model density* profile ρ is obtained using a four-parameter linear model fit to the estimated density profile described above. Because this model describes the density profile in such a way that excludes localized wave structure, scale heights and peak densities may be obtained from the model densities.

This density recovery process will be described in detail in the following sections.

Estimated Density

Freestream atmospheric density along the spacecraft trajectory may be recovered directly from the spacecraft accelerations by utilizing Newton's Second Law and the definitions of dynamic pressure and the aerodynamic force coefficients[1-5], such that

$$\hat{\rho}_\infty = \frac{2ma_x}{V_\infty^2 C_A S} \tag{3}$$

where m is the spacecraft mass, a_x is the axial acceleration, V_∞ is the freestream velocity, C_A is the axial force coefficient, and S is the spacecraft reference area. The value of spacecraft mass is updated periodically as fuel is consumed. The freestream velocity is computed from the spacecraft state (position and velocity), which is obtained from orbital elements at periapsis provided by the MAVEN Orbit Propagation Timing and Geometry file (OPTG).[14] The orbital elements are propagated forwards and backwards from time of periapsis assuming a Keplerian orbit and converted to Cartesian position and velocity components in the inertial frame. These inertial state vectors are then mapped into the spacecraft body-fixed frame using the direction cosine matrix that transforms between the inertial frame to the body-fixed frame and the rotation rate of the planet.

In previous aerobraking mission analyses[1-5], which had the same orientation to the wind across each periapsis pass, only the component of acceleration along the velocity vector was considered in determining density. For example, MRO was flown with the body *y*-axis into the wind, and thus the acceleration *y*-component exhibited the largest signal-to-noise ratio. Eq. 3 uses the *x*-component of acceleration and the axial force coefficient, and therefore is appropriate for application to a spacecraft with the *x*-axis pointing into the wind. Because MAVEN flies at different attitudes through periapsis for any given orbit, the present work modifies this approach to use all three acceleration components simultaneously, meaning that the acceleration of the spacecraft CG due to aerodynamic drag from Eq. (2) is used (the CG subscript is dropped for clarity):

$$a_d = \mathbf{u} \cdot \mathbf{a} = u_x a_x + u_y a_y + u_z a_z \tag{4}$$

where $\mathbf{u}$ is the wind-relative vehicle velocity unit vector and $\mathbf{a}$ is the aerodynamic acceleration vector, both expressed in the spacecraft aerodynamic frame. The drag coefficient is obtained from the wind-relative velocity unit vector in the spacecraft body frame and the corresponding aerodynamic coefficients:

$$C_d = u_x c_x + u_y c_y + u_z c_z \tag{5}$$

Thus, dropping the freestream notation, the atmospheric density is estimated by

$$\hat{\rho} = \frac{2ma_d}{V^2 C_d S} \tag{6}$$

Model Density

Eq. (6) provides the density estimate at any time along the trajectory. Thus, any local variations in the atmosphere that can be detected by accelerometers, such as gravity waves, will be reflected in the resultant estimated density profile. These local variations will preclude accurate recovery of scale heights or peak density. For this reason, a model is used to predict a density bell curve that reflects a typical density profile:

$$-\rho = e^{\left(C_1 + C_2 t_p + C_3 h + C_4 t_p h\right)} \tag{7}$$

where $C_{1..4}$ are the model coefficients, t_p is the time since periapsis, and *h* is the corresponding altitude. In this form, which is used for the low-density science orbits, the coefficients are determined using a non-linear estimation method and the data may include negative densities, i.e., data noise. The coefficients may be interpreted in terms of density variations: C_1 determines the density at periapsis, C_2 is an indicator of along-track density gradients at periapsis altitude, C_3 is inversely proportional to the traditional density scale height, and C_4 is an indicator of the along-track gradient in density scale height or temperature. Since in the vicinity of periapsis, *h* is proportional to t_p^2, the model is essentially the first four terms in the Taylor series expansion for $\log\rho$ and therefore unacceptable for extrapolation beyond the few hundred seconds about time of periapsis.

For DD orbits, only the central peak of the profile is fit with the model, providing all positive measurements. Consequently $\log\rho$ can be used as the measurement set and Eq. (7) reduces to a linear estimation problem that is solved using the classical least squares estimator

$$\mathbf{y} = \mathrm{A}\mathbf{x} \tag{8}$$

where **y** is a vector of the *n* values of $\log\rho$, **x** is the vector of the model coefficients C_1 through C_4, and A is the sensitivity matrix that relates the estimated parameters **x** to the observations **y**. The covariance of **x** is then

$$\Gamma_{\mathrm{x}} = \sigma^2 \left(\mathrm{A}^{\mathrm{T}}\mathrm{A}\right)^{-1} \tag{9}$$

where σ^2 is the variance of the residuals between the model and data. The diagonals are the squared standard deviations of the model coefficients:

$$\mathrm{diag}\left(\Gamma_{\mathrm{x}}\right) = \begin{bmatrix} \sigma_{C_1}^2 & \sigma_{C_2}^2 & \sigma_{C_3}^2 & \sigma_{C_4}^2 \end{bmatrix}^{\mathrm{T}} \tag{10}$$

Various atmospheric parameters may then be recovered from the model coefficients provided by Eq. (8). The model density profile is provided by Eq. (7). The density and scale height at periapsis are

$$\rho_p = \exp\left(C_1\right) \tag{11}$$

$$H_s = -1/C_3 \tag{12}$$

The model density and scale height uncertainties at periapsis are computed using the standard deviations from Eq. (10). These uncertainties may be interpreted as descriptions of the quality of the model fit.

RESULTS

The density estimation and atmospheric parameter recovery process described in previous sections was applied to MAVEN accelerometer data during both nominal science and DD campaign operations.

Nominal Science Orbits

Figure 8 show areodetic altitudes and estimated and model densities of typical science orbits. The estimated density profile $\hat{\rho}$ provided by Eq. (6) is shown in blue, the model density profile ρ provided by Eq. (7) is shown in red, and the areodetic altitude profile is shown in dashed black. The left panels of each sub figures show densities and areodetic altitudes as a function of time from periapsis where periapsis occurs at 0.0 s. The uncertainty of the model density in a 1σ sense is printed in the left panel titles. The right panels show the of log density as a function of areodetic altitude. The slope of the model density provides the scale height at altitudes near periapsis, printed on the plots near the minimum density with the associated uncertainty.

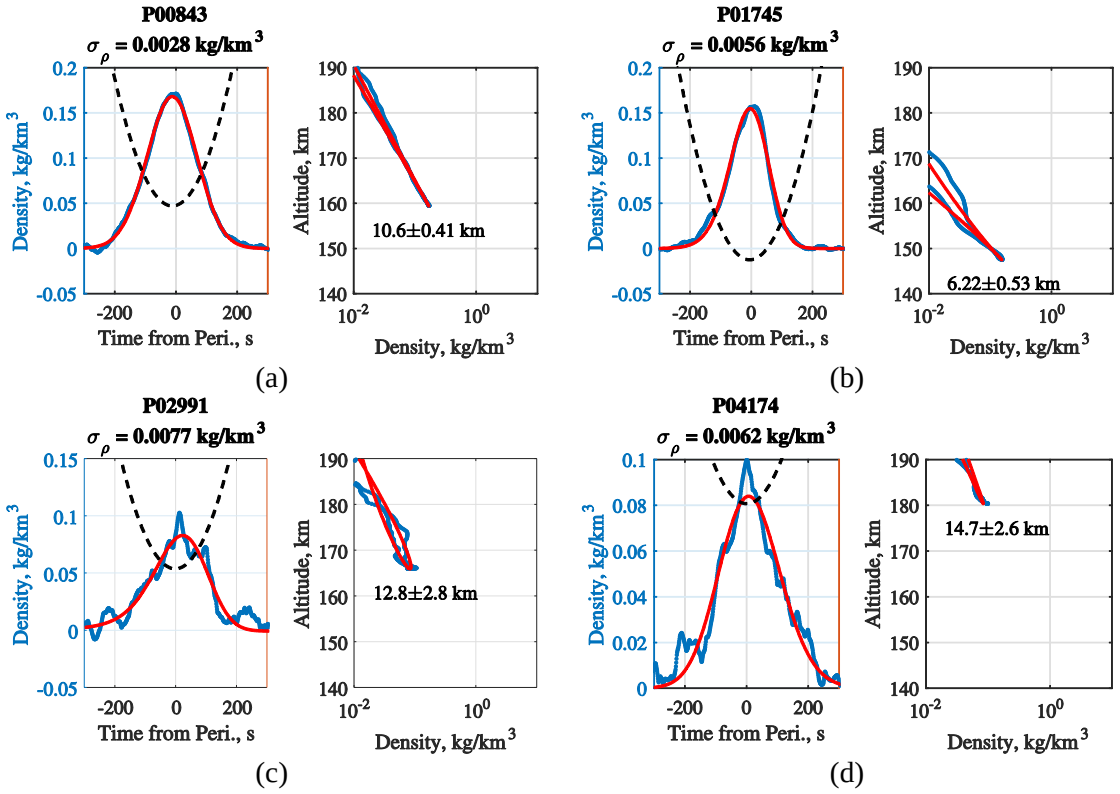

Figure 8. Selected science orbit densities and model fits, (a) Orbit 843, (b) Orbit 1745, (c) Orbit 2991, (d) Orbit 4174.

For orbits 843 and 1745 (denoted in Figure 8 as P00843 and P01745, respectively), the peak density is just over 0.15 kg/km^3 and occurs very near periapsis. The inbound and outbound profiles for orbit 843 are nearly identical, and with the peak at periapsis would be well-modeled by the traditional isotheral and hydrostatic constant scale height profile. Orbit 1745 provides an example

in which inbound and outbound profiles differ but the peak is still near periapsis. The model can fit this type of variation by introducing the along-track scale height gradient. This orbit also exhibits a "dip" at approximately -160 s that is characteristic of a gravity wave. Note the noisy signal at densities near zero, including some negative densities, which is indicative of accelerometer measurement noise corrupting the density estimates. Orbits 2991 and 4174 both have peak densities at or below 0.10 kg/km^3 (note the high minimum altitudes of 165 km and 180 km, respectively). These orbits show estimated density profiles that are quite noisy through periapsis due to limits in the accelerometer measurement capability, compared to the previous orbits. It is unlikely that any structure seen in these orbits is real, aside from the characteristic bell curve.

Though in general it is difficult to draw definitive conclusions from reconstructions of individual orbits such as these due to noise, analyzing many orbits at once may provide additional insight. Thus, an analysis of medium-term trends and comparisons to NAV during nominal science orbits was also conducted. Figure 9 shows drag ratio, model density at time of periapsis, and periapsis scale height variations and comparisons between ACC and NAV for science orbits 3665-4174, covering a period between August 15th, 2016 and November 21st, 2016 (approximately 99 days). This range of dates was selected because it highlights several notable features.

The mean drag ratio between ACC and NAV across all orbits (top panel) is 1.19. This is consistent with the difference in surface gas interaction assumptions between the LMSSC aerodatabase and the aerodatabase developed and used by the accelerometer group (refer to the previous discussion in this paper on the spacecraft aerodynamic database).

There is a significant, sudden drop in periapsis density just prior to orbit 3915, corresponding to a spacecraft up-maneuver. There is also a noticeable, out-of-family drop in the drag ratio starting at orbit 4146 and continuing to orbit 4156. These orbits correspond to an IUVS stellar occultation experiment that required the spacecraft to slew through different attitudes during the periapsis pass.

In general, scale height variability is high. However, there is a region of notably low variability between orbits 3865 and 3915, corresponding to densities above 0.1 kg/km^3. While this low variability may be attributed to the high density, another region, between orbits 3715 and 3765 exhibits high densities but high scale height variability.

Ultimately, despite orbit-to-orbit variations, there is overall good agreement between ACC and NAV periapsis density trends.

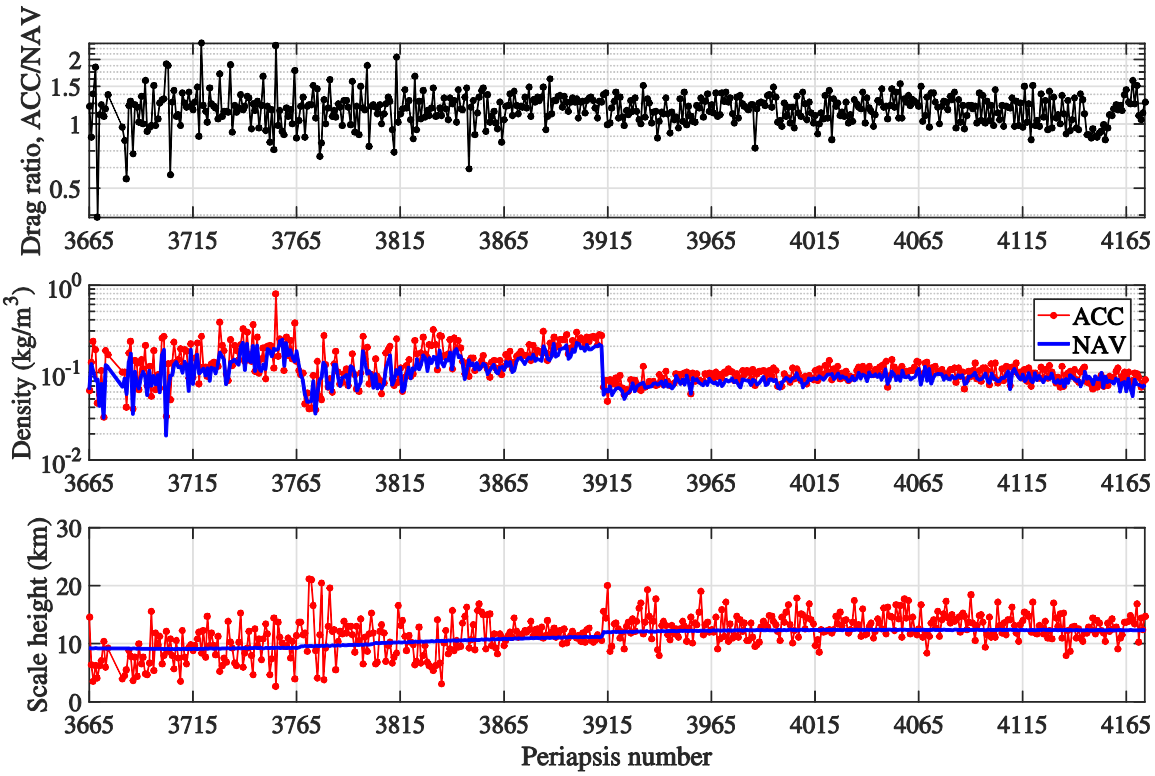

Figure 9. Drag ratio, model density at time of periapsis, and periapsis scale height variations and comparisons between ACC and NAV.

Deep Dip Orbits

Figure 10 shows areodetic altitudes, and estimated and model densities of typical orbits in various DD campaigns. As in Figure 8, the estimated density profile $\hat{\rho}$ provided by Eq. (6) is shown in blue, the model density profile ρ provided by Eq. (7) is shown in red, and the areodetic altitude profile is shown in dashed black. The uncertainty of the model density in a 1σ sense is printed in the left panel titles. The altitude ranges used to compute scale heights at the 150 km reference altitude are shown in black, with the values of inbound and outbound scale height printed in the right panel titles.

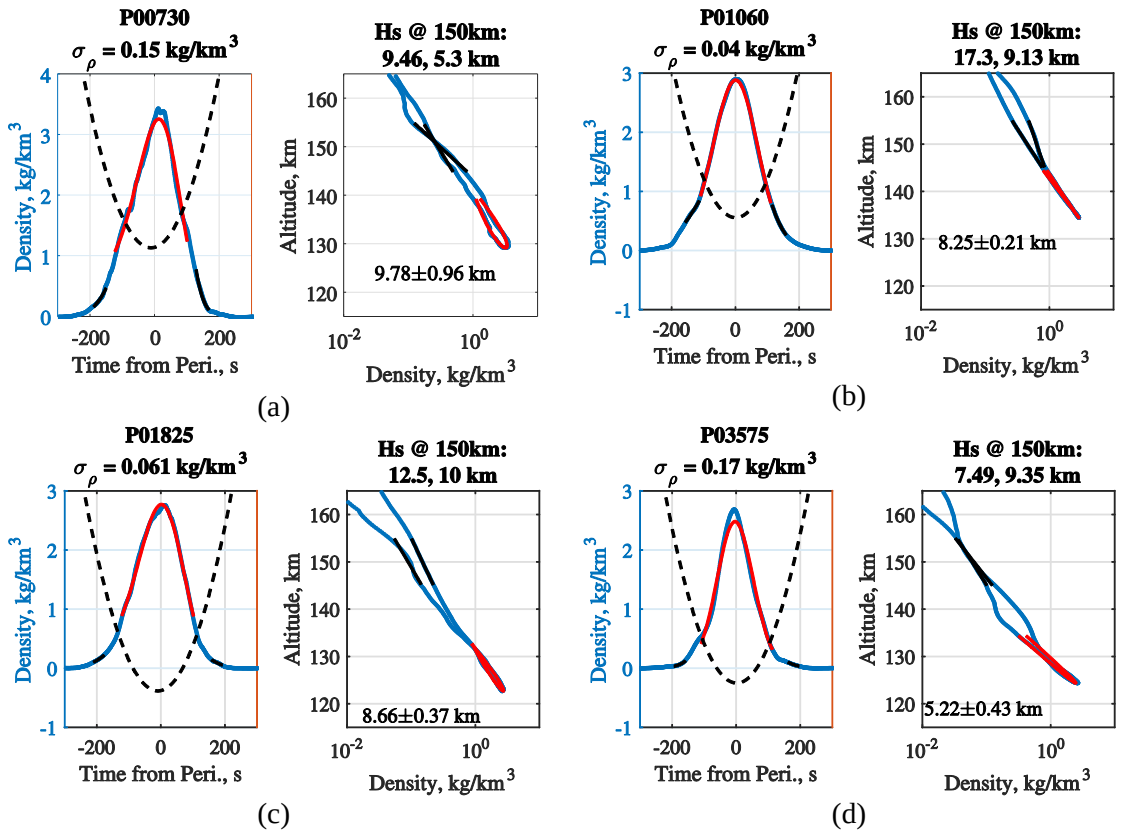

Figure 10. Selected Deep Dip orbit densities and model fits, (a) Orbit 730, DD1, (b) Orbit 1060, DD2, (c) Orbit 1825, DD4, (d) Orbit 3575, DD6.

Compared to Figure 8, the density profiles shown here exhibit peak densities in keeping with the DD density corridor requirements. Some wave structure can be seen that prevents the model from capturing the peak density of orbits 730 and 3575, but otherwise the model fits the estimated density profiles well. The peak density in orbit 730 occurs after time of periapsis, which is absorbed by the model in the along-track density gradient. Orbit 1825 shows the inbound and outbound profile crossing near periapsis near 132 km. In the model, this type of variation is represented by an along-track scale height gradient. The scale heights at the reference altitude of 150 km show that there can be significant variance between the inbound and outbound segments of the density profiles.

The left panel of Figure 11 shows the variation of periapsis altitudes during each DD campaign. The circled data points are orbits that were expected to be in the targeted density corridor; i.e., the actual DD orbits. The data points that are not circled illustrate the periapsis lower (walk-in) and raise (walk-out) maneuvers. The right panel of Figure 11 shows the variation of periapsis density estimates recovered from Eq. (6) with the same orbits as circled in the left panel. Note the high variability of the periapsis densities compared to the variability of the corresponding periapsis altitudes. Of particular note is Deep Dip 6 (DD6), which exhibited both the highest and lowest periapsis densities of any DD campaign. Further discussion of the science implications from these results is available in Zurek *et al*., 2017.[15]

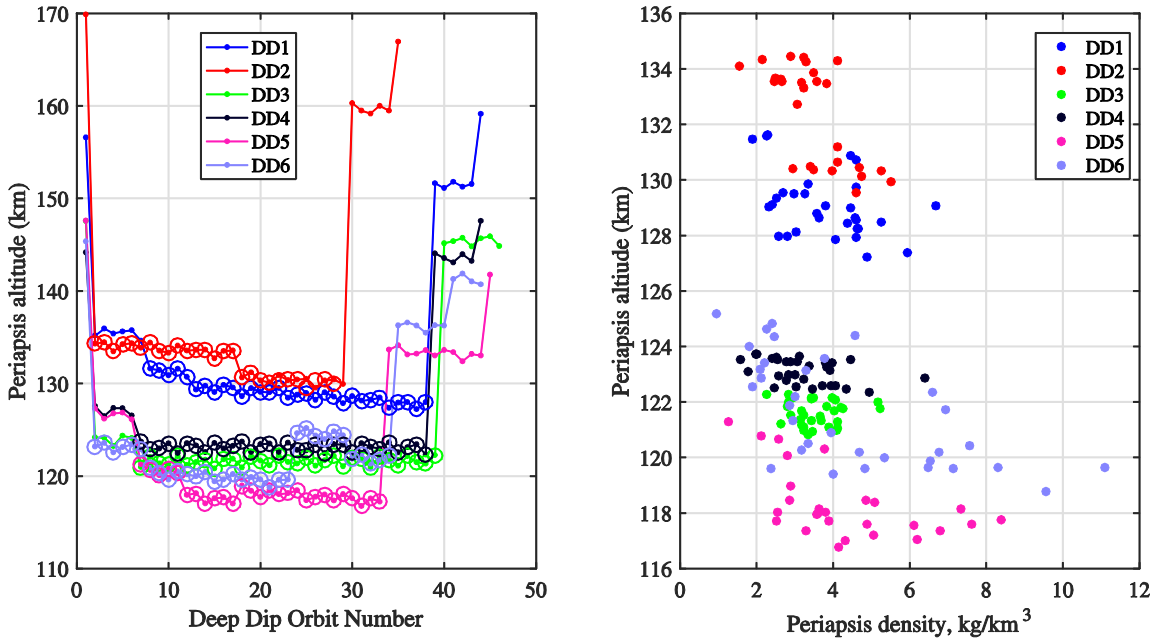

Figure 11. Periapsis altitudes and densities of orbits in Deep Dips 1-6.

SUMMARY AND CONCLUSIONS

A modification of an existing method to recover atmospheric density from spacecraft accelerometer data has been presented. The modified method utilizes all three accelerometer data channels rather than the one that exhibits the highest signal-to-noise ratio, as was done on previous Mars orbiter missions. An exponential model is used to recover scale heights and gradients. The modified method is applied to accelerometer data from the MAVEN mission and results compared to navigation-derived peak densities and scale heights. Though there is orbit-to-orbit variability, there is good agreement in medium-term trends, and good agreement in Deep Dip orbits. This modified method will continue to be applied to MAVEN accelerometer data through its extended mission.

ACKNOWLEDGEMENTS

The authors thank Stuart Demcak (JPL), Wayne Sidney, and Mark Johnson (LMSSC) for providing spacecraft operation and navigation updates and information. This work was sponsored by the MAVEN program at the NASA Goddard Space Flight Center and the Jet Propulsion Laboratory at the California Institute of Technology.

NOTATION

ACC	Accelerometer
ACS	Attitude control system
CG	Center of gravity
CM	Center of mass
DAC	DSMC Analysis Code
DD	Deep Dip
DSMC	Direct Simulation Monte Carlo
LMSSC	Lockheed Martin Space Systems Company
MAVEN	Mars Atmosphere and Volatile EvolutioN

MarsGRAM	Mars Global Reference Atmospheric Model
MGS	Mars Global Surveyor
MIMU	Miniature inertial measurement unit
MOI	Mars orbit insertion
MRO	Mars Reconnaissance Orbiter
NAV	Navigation group
ODY	Mars Odyssey
OPTG	Orbit Propagation Timing and Geometry
SDC	Science Data Center
A	Sensitivity matrix
C_1, C_2, C_3, C_4	Model coefficients
C_d	Drag coefficient
H_s	Scale height
S	Spacecraft reference area
V_∞	Freestream velocity
a_d	Acceleration due to aerodynamic drag
a_x, a_y, a_z	Acceleration vector
c_x, c_y, c_z	Aerodynamic coefficients
h	Altitude
m	Spacecraft mass
r	Spacecraft CG position vector
t_p	Time since time of periapsis
u_x, u_y, u_z	Spacecraft velocity unit vector
x	Vector of model coefficients
y	Vector of *n* values of $\log \rho$
Γ_x	Covariance of **x**
ρ	Density
σ	Standard deviation
ω	Spacecraft angular velocity vector

REFERENCES

[1] Tolson, R. H., et al., "Application of MGS and ODY Aerobraking Accelerometer Data to Atmospheric Modeling," AIAA 06-6397.

[2] Tolson, R. H., et al., "Application of Accelerometer Data to Mars Odyssey Aerobraking and Atmospheric Modeling," AIAA 02-4533.

[3] Tolson, R. H., et al., "Atmospheric Modeling Using Accelerometer Data During Mars Reconnaissance Orbiter Aerobraking Operations," AAS 07-183.

[4] Tolson, R. H., et al., "Application of Accelerometer Data to Atmospheric Modeling During Mars Aerobraking Operations," *Journal of Spacecraft and Rockets*, Vol. 44, No. 6, November-December 2007, pp. 1172-9.

[5] Zurek, R.W., Tolson, R. H., Baird, D. T., Johnson, M. Z., and Bougher, S. W., "Application of MAVEN Accelerometer and Attitude Control Data to Mars Atmospheric Characterization," Space Sci. Rev., DOI 10.1007/s11214-014-0095-x.

[6] Jakosky, B. M., et al., "Initial results from the MAVEN mission to Mars," *Geophys. Res. Lett.*, Vol. 42, pp 8791-802.

[7] Jesick, M., et al., "MAVEN Navigation Overview," AAS 16-237.

[8] Demcak, S., et al., "MAVEN Navigation During the First Mars Year of the Science Mission," AIAA 2016-5428.

[9] "The MAVEN Spacecraft," NASA, URL: https://www.nasa.gov/mission_pages/maven/spacecraft/index.html [cited 15 December 2016].

[10] Waters, Chris, "Coordinate Systems Definition Document," Lockheed Martin Space Systems Company, 18 May 2012, MAV-RP-10-0100 Rev D.

[11] "The MAVEN Science Data Center," URL: http://lasp.colorado.edu/home/maven/2012/08/27/the-maven-science-data-center [cited 19 September 2016].

[12] "DSMC Code Simulates Rarefied Gas Dynamic Environments," NASA Johnson Space Center, URL: https://www.nasa.gov/centers/johnson/techtransfer/technology/MSC-23445-1-dsmc-dac.html [cited 15 December 2016].

[13] Fuller, J. and Tolson, R., "Improved Method for the Estimation of Spacecraft Free-Molecular Aerodynamic Properties," *Journal of Spacecraft and Rockets*, Vol. 46, No. 5, September-October 2009, pp. 938-48.

[14] "Detailed Explanation of OPTG Files," Jet Propulsion Laboratory, URL: http://mars.jpl.nasa.gov/mgs/jpl-telem/optgex.html [cited 20 September 2016].

[15] Zurek, R. W., Tolson, R. A., Bougher, S. W., Lugo, R. A., Baird, D. T., Bell, J. M., and Jakosky, B. M., "Mars Thermosphere as seen in MAVEN Accelerometer Data," *Journal of Geophysical Research*, 2017, to be published.